Modelling of Real Shear Thickening Fluid (STF) Flow around a Circular Cylinder within a Channel using the Lattice Boltzmann Method

Garima Vishal, **Ashish Garg**, **Jayati Sarkar***, **Sudip K. Pattanayek***,
Department of Chemical Engineering, Indian Institute of Technology Delhi, India

January 11, 2024

Abstract

A real shear thickening fluid (STF) exhibit a complex combination of Newtonian and non-Newtonian behavior, including shear thinning and shear thickening viscosity-shear rate profile. Understanding the flow dynamics of STFs through intricate geometries, particularly in confined spaces, is crucial for the development of impact-resistant systems. To explore the flow characteristics of the real shear thickening fluids over cylindrical surface confined in a channel, we employed the Lattice Boltzmann method (LBM) within a D2Q9 framework for mesoscopic numerical simulations. The velocity and pressure profiles has been explored to the limit so that effect of real STF can been explored. Our finding are focused on the real STF effects near the cylinder and how it varies with the Reynolds number. We find that the Real shear thickening fluids exhibit a complex changes in the wake flow pattern as compared to Newtonian, power-law shear-thinning and thickening fluids. In case of Real STF, due to low shear rates, we find thinning behaviour near the centerline of the channel (i.e., in the core) of the flow where the cylinder is placed. Hence, the vortex shedding and recirculation is less intense as compare to the power-law Shear Thickening Fluid (STF) and Newtonian flows. We also find that the Real shear thickening fluid flow is more accelerated onto the cylinder and exhibit early separation as compared to the thickening or Newtonian fluid, thereby creates more pressure drag as compared to the Newtonian and pure power-law thickening fluids, whereas due to low viscosity onto the cylinder it creates less skin drag as compared to the Newtonian and pure power-law thickening fluids.

Keywords: Combining shear thickening and thinning flow behaviour, Lattice Boltzmann method, Shear thickening Fluid, wake flow in channel, flow on a cylinder, Real shear thickening fluids.

*Email: **sudip@chemical.iitd.ac.in, jayati@chemical.iitd.ac.in**

1 Introduction

Flow past a cylinder is a classic problem in fluid dynamics, and is extensively studied geometry for flow of Newtonian fluids and non-Newtonian fluids. The flow geometry is also important in understanding the flow behaviour of a real fluid in some practical applications like development of soft body armour, damping and vibration control, industrial gloves and dampers etc. In these applications, the real shear thickening fluid used [1–3] follows the combination of Newtonian, shear thinning and shear thickening behaviour as shear rate changes.

There are considerable number of literature on the flow of single type of fluid (i.e. Newtonian, shear thinning or shear thickening) over cylindrical geometry in 2D [4–13] and 3D [14] using computational fluid dynamics (CFD), or with Lattice Boltzmann methods(LBM)[15]. We note that there is development of the analytical work on the flow in the above geometries of flowing fluids obeying Newtonain or power law models [5]. Perumal et al. [13] have used the Lattice Boltzmann Method (LBM) to study the flow field characteristics of Newtonian fluids over elliptical cylinder at various Reynolds numbers. The frequency of vortex shedding is found to be contingent on factors like end conditions and blockage ratio within the flow passage. Additionally, the study explores the impact of key parameters on the characteristics of vortex shedding. Grucelski and Pozorski [16] have used multi relaxation lattice Boltzmann method, (MRLBM) to incorporate the marginally superior stability and accuracy in case of Newtonian fluid flow past a cylinder, provided that the associated higher numerical cost is deemed acceptable. While reasonable accuracy can be attained through the application of (non-equilibrium) half-way bounce-back conditions, it is advisable to consider alternative conditions, such as the interpolation-free scheme, particularly for variable geometries. Yan and Zu [17] conducted a study on the impact of Reynolds number and Prandtl number. They examined the velocity profile for flow separation at a specific normalized time (dimensionless).

Nejat et al. [15] studied the flow past a cylinder for non Newtonian fluids obeying power law model using single relaxation lattice Boltzmann method. They reported that the drag coefficient exhibits a slightly nonlinear amplification with an increase in the Power-Law index that is from shear thinning ($n < 1$) to Newtonian ($n = 1$) to shear thickening ($n > 1$). This outcome was anticipated, as a higher Power-Law index corresponds to increased shear, resulting in larger drag. Additionally, the pressure drag coefficient decreases as the power-law index ($n = 0.4$ to $n = 1.6$) rises, at a constant Reynolds number. Fallah et al. [18] have studied the shear thinning and shear thickening fluids which follow the power law model where power law index varies from 0.4 to 1.8 using multi relaxation time lattice Boltzmann method. It revealed that as the power law index increases, both the length and width of the wake also experience an increase. Bisht and Patil [19] explored the Multiple relaxation time lattice Boltzmann method (MRT-LB) framework to study several non-Newtonian fluid models, including Power-law, Carreau,

Carreau–Yasuda, and Cross, in the context of a two-dimensional benchmark problem involving flow past a cylinder. The drag coefficient (Cd) is computed using these viscosity models and is compared with literature values, indicating a favorable agreement. In addition to it, a cascaded lattice Boltzmann (LB) formulation [20], utilizing central moments and multiple relaxation times, has been devised for solving non-Newtonian fluid flow models. It has been observed that as the Reynolds number (Re) increases, while keeping the power law index (n) constant, the drag coefficient decreases.

The majority of research has concentrated on investigating the critical Reynolds number, drag coefficent and wake formation across various channel diameters for both Newtonian and non-Newtonian fluids. However, there is a notable gap in the literature regarding the examination of the flow behavior of real shear-thickening fluids. This paper aims to address this gap by delving into the flow characteristics of a real shear-thickening fluid in the context of flow past a cylinder. Here we have used Multi relaxation time Lattice Boltzmann method (MRT-LBM) method to do the numerical calculations and compared a few results to the existing results in literature and our analytical analysis. We are focusing on MRT-LBM because it provides more stability to the variation of viscosity which mean MRT can work in the larger ranges of viscosity. Here we have explored various aspects of flow behavior such vortex shredding, pressure and coefficients and drag forces.

2 Model Description

In the context of fluid dynamics, we are investigating the flow of fluid past a cylinder within a channel. The domain under examination has specific dimensions: the length of the domain (L) measures 600 lu (length units), while the height of the domain (H) is 80 lu. This results in an L/D ratio of 10, indicating that the channel is ten times longer than it is wide, effectively allowing for a two-dimensional flow around the cylinder. A parabolic velocity profile has been considered to effectively allowing for a two-dimensional flow around the cylinder [5]. The diameter of the cylinder (d) is 20 lu, which gives us a H/d ratio, often referred to as the wall blockage ratio, of 4. This configuration serves as a standard benchmark problem in fluid dynamics and is commonly referred to as flow past a cylinder in a channel flow.

Researchers employ such standardized setups to explore various aspects of flow behavior, including phenomena such as wake formation and boundary layer separation, facilitating consistent comparisons and validations across different studies. We have tried to study the real shear thickening fluid (STF) through this setup. A real STF is a non Newtonian fluid exhibits distinct regions of Newtonian behavior, shear thinning, and shear thickening when plotted on the viscosity-shear rate graph. To investigate the flow properties of such a fluid, we utilized the Lattice Boltzmann method (LBM) within a D2Q9 framework, employing mesoscopic simu-

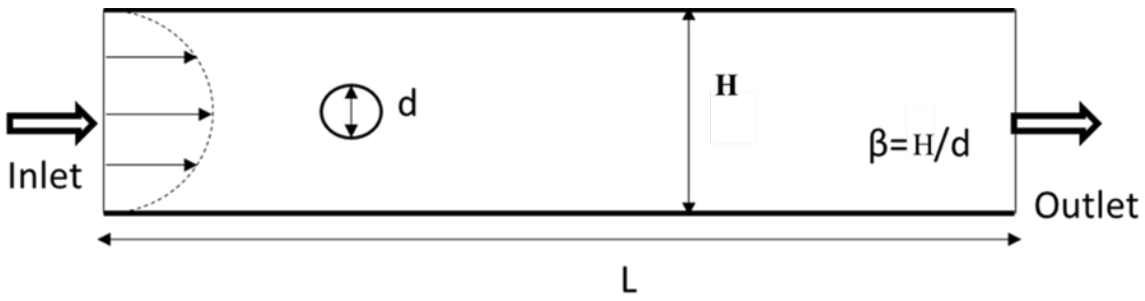

Figure 1: Schematic diagram of the domain

lations.

We applied the Lattice Boltzmann method (LBM). The steps of LBM are initialization, equilibrium calculation, collision step, streaning stem, boundary condition and macroscopic variable. All these steps are discussed in detail [21]. To gain insights into LBM, relevant references can be found in papers [21, 22]. Our approach aligns with the methodology detailed in these papers, with a key modification in the boundary treatment at the cylinder wall. The cylinder geometry was constructed in a step manner, and the no-slip condition was enforced at the wall using the bounce-back method, as described by the following equation in terms of distribution function.

$$f_2(i,0,t+\Delta t) = f_4^*(i,0,t^+) \tag{1}$$

$$f_5(i,0,t+\Delta t) = f_7^*(i,0,t^+) \tag{2}$$

$$f_6(i,0,t+\Delta t) = f_8^*(i,0,t^+) \tag{3}$$

$$f_4(i,N-1,t+\Delta t) = f_2^*(i,N-1,t^+) \tag{4}$$

$$f_7(i,N-1,t+\Delta t) = f_5^*(i,N-1,t^+) \tag{5}$$

$$f_8(i,N-1,t+\Delta t) = f_6^*(i,N-1,t^+) \tag{6}$$

2.1 Boundary Conditions :

We have used fully developed velocity inlet and pressure outlet condition at the boundaries. At curved boundary the cylinder in the channel has no slip boundaries conditions. The details are given in figure 2.

In figure 2 we have given the details of the boundary condition used in the channel. In figure 2(A) the distribution functions are given for inlet and outlet where the unknown density function are calculated using equation given in [21]. In figure 2(B) the curved boundary treatment for cylinder is given and the below given equation are utilised to give bounce back boundary condition. The cylinder geometry was constructed in a step manner as given in figure 2(B), and

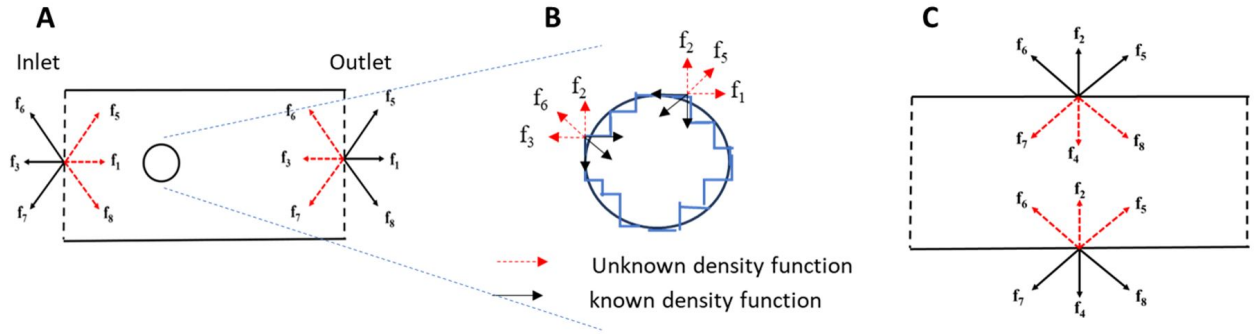

Figure 2: Distribution functions at boundaries (A) Inlet and outlet (B) wall of the cylinder (C) wall of the channel

the no-slip condition was enforced at the wall using the bounce-back method, as described by the following equation in terms of distribution function.

$$f_2(i,j,t+\Delta t) = f_4^*(i \pm 1, j \pm 1, t^+) \tag{7}$$

$$f_5(i,j,t+\Delta t) = f_7^*(i \pm 1, j \pm 1, t^+) \tag{8}$$

$$f_6(i,j,t+\Delta t) = f_8^*(i \pm 1, j \pm 1, t^+) \tag{9}$$

$$f_1(i,j,t+\Delta t) = f_3^*(i \pm 1, j \pm 1, t^+) \tag{10}$$

In figure 2(C) the top and bottom boundary wall treatment is given where no slip boundary condition is utilised. Applying the Lattice Boltzmann method, as detailed in the referenced paper (24), and incorporating the specified boundary conditions, we successfully addressed the problem. The ensuing section presents the obtained results. The inlet velocity and pressure outlet boundary conditions has been used. The power law model of viscosity is defined

$$\eta = m|\dot{\gamma}|^{n-1} \tag{11}$$

Where η is the viscosity and n is power law index and m is the consistency index. It is also worth mentioning that if $n < 1$, the shear thinning fluid can be modelled, if $n = 1$, the Newtonian fluid can be modelled and if $n > 1$, the shear thickening fluid can be modelled. Reynolds number (Re) for a power law fluid flowing through the channel of height and circular cylinder of diameter d is given by

$$Re = \frac{12\ \rho\ u_{avg}^{(2-n)}\ d^n}{m\ (2+1/n)^n}, \tag{12}$$

where, ρ is the density and u_{avg} is the average velocity, n is the power law index m is the consistency index. Calculating the Reynolds number for the Real Shear thickening fluid flow is not possible hence we need parameters where n is not required. In this scenario the following parameters play a crucial role [23].

Drag Coefficient: It is the resistance provided to the flow by the fluid. The drag coefficient which is a dimensionless number can be given by the following equation

$$C_d = F_D/(0.5\ \rho\ u_{max}^2), \tag{13}$$

where F_D is the drag force, ρ is the density and u_{max} is the maximum velocity.

Pressure coefficient C_p: It is given by the following equation

$$C_p = \frac{2(p_{\text{cylinder}}(\theta) - p_{\text{centreline}})}{\rho_{\text{centreline}} U_{\text{centreline}}^2}, \tag{14}$$

where C_p and $p_{\text{cylinder}}(\theta)$ refer to the pressure coefficient and the pressure value at a certain angle on the cylinder. Also, from the inviscid, incompressible, potential theory, the pressure coefficient for the flow on the cylinder is given by $C_p = 1 - 4\sin^2(\theta)$ [24]. In the next section we are going to understand more about the fluid flow behaviour.

3 Results and discussions

In our initial validation process, we focused on calculating the drag coefficient and comparing it to existing literature data. Specifically, we examined the case of Reynolds number Re= 40 for both Newtonian and non-Newtonian fluids. The drag coefficient is a critical parameter in fluid dynamics as it quantifies the resistance experienced by an object moving through a fluid. The drag coefficient can be given by the following equation

$$C_d = F_D/(0.5\ \rho\ u_{max}^2) \tag{15}$$

Where F_D is the drag force, ρ is the density and u_{max} is the maximum velocity. Upon conducting our calculations and comparing the results with data available in the literature, we observed a strong agreement between our findings and the established values reported in previous studies. This agreement indicates that our computational model and methodology are consistent with established research standards and are capable of accurately predicting the drag coefficient for this particular flow scenario. Overall, this successful match between our results and the literature findings provides a solid foundation for our further investigations and lends credibility to our computational approach in studying fluid flow around the cylinder in a channel. It signifies that our simulations are producing reliable and comparable results with (7,28), which is a crucial step in any research involving fluid dynamics.

3.1 Newtonian fluid Flow

We find the initiation of wake instability, marking the transition from a two-dimensional 'symmetric' (as shown in Figure 3a.(i)) to an 'asymmetric' (as shown in Figure 3.a(ii)) wake flow

	C_d, $n = 1$	C_d, $n = 1.2$
Bharti et al. [8]	1.7034	1.8793
Bijjam and Dhiman [5]	1.7039	1.8781
Present work	1.717	1.8227

Table 1: Comparison of drag coefficient values for steady power-law fluid flow over a cylinder for Reynolds number 40 and $\beta = H/d = 4$

	Given		**Calculated**	
Case	n	m	Re	ΔP
(i)	1	0.03	45.7	-0.007
(ii)	1	0.025	57.1	-0.015

Table 2: Defining the case study with the symbol (i) and (ii) form different viscosity $\eta = m|\dot{\gamma}|^{n-1}$

regime, as determined by the range of Reynolds number (Re) from 45.7 to 57.1. We complement this analysis by visualizing streamline profiles and examining the drag coefficient (C_d) over the cylinder. These assessments help us pinpoint the shift from a stable, steady 'symmetric' flow to an 'asymmetric' flow pattern.

Our initial analysis focused on investigating the instability of Newtonian fluid by altering its viscosity, consequently leading to variations in the Reynolds number. Our primary objective in this investigation was to assess how changes in fluid viscosity influence the stability of the flow. This examination sheds light on the crucial relationship between fluid properties and flow stability, contributing to our understanding of fluid dynamics in this context.

In Figure Figure 3(a), we present velocity contours for both case (i) and case (ii), offering significant insights into the flow behavior under different conditions. In case (i), the contours reveal a stable flow pattern characterized by a symmetric wake formation. However, in case (ii), distinct signs of flow instability become apparent, accompanied by the emergence of a vortex shedding phenomenon. This observation indicates that the flow undergoes a transition from stability to instability within the Reynolds number range of 45.7 to 57.1. This shift in flow behavior underscores the sensitivity of the system to changes in Reynolds number, providing valuable data for understanding the onset of instability. Figure 3(b) showcases pressure contours for both cases (i) and (ii), providing crucial insights into the pressure distribution along the flow direction. In case (i), the contours reveal a gradual and consistent decrease in pressure as the flow progresses. This gradual reduction in pressure is indicative of a well-behaved, stable flow pattern, where the fluid moves smoothly around the cylinder, and the pressure distribution follows a predictable trend. Conversely, in case (ii), a distinct difference emerges. The pressure contours exhibit a non-gradual variation in pressure along the flow direction. This departure

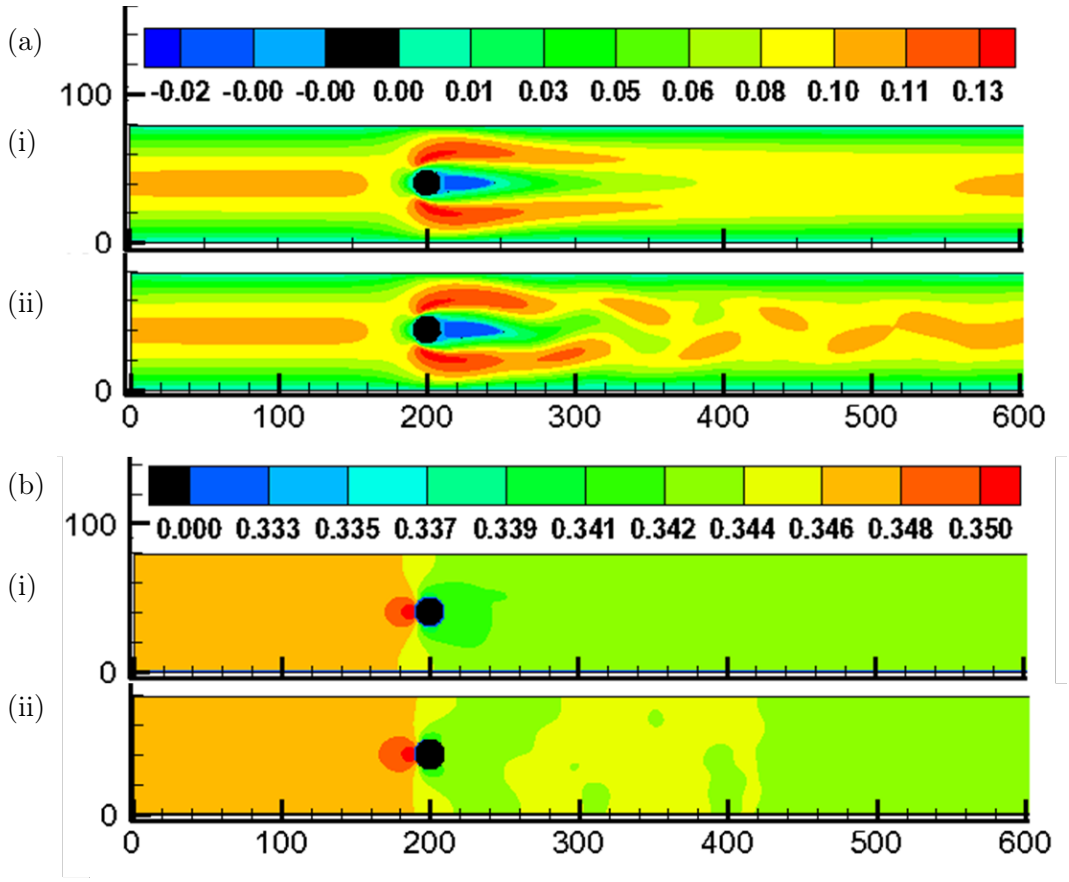

Figure 3: Contour plots for Newtonian fluid (a) Velocity contour (b) Pressure contour

from a gradual pressure decrease suggests a disruption in the flow behavior. Specifically, it indicates that the flow in case (ii) is experiencing instability or turbulence, leading to irregular pressure distributions. This observation aligns with our earlier assessment of instability in case (ii), where vortex shedding was detected. The non-gradual pressure changes in case (ii) further emphasize the turbulent nature of the flow, highlighting the impact of flow instability on pressure patterns along the cylinder's path. These findings are essential for comprehending the dynamic changes occurring in the wake of the cylinder and contribute to a comprehensive understanding of fluid flow behavior in this context.

3.2 Shear-thinning fluid Flow

In this section, we discuss, Shear-thinning fluid flows. The discussed viscosity profiles are given in table 3. Figure 4(a) presents velocity contours for both case (i) and case (ii), providing significant insights into the flow characteristics. In case (i), a clear and symmetrical flow profile is evident, indicating stable flow behavior. Conversely, in case (ii), an asymmetrical flow pattern

	Given		Calculated	
Case	n	m	Re	ΔP
(i)	0.7	0.007	34.6	-0.007
(ii)	0.7	0.006	40.7	-0.01

Table 3: Defining the case study with the symbol (i) and (ii) form different viscosity. Case (i): $n = 0.7, m = 0.07$, Case (ii): $n = 0.7, m = 0.06$

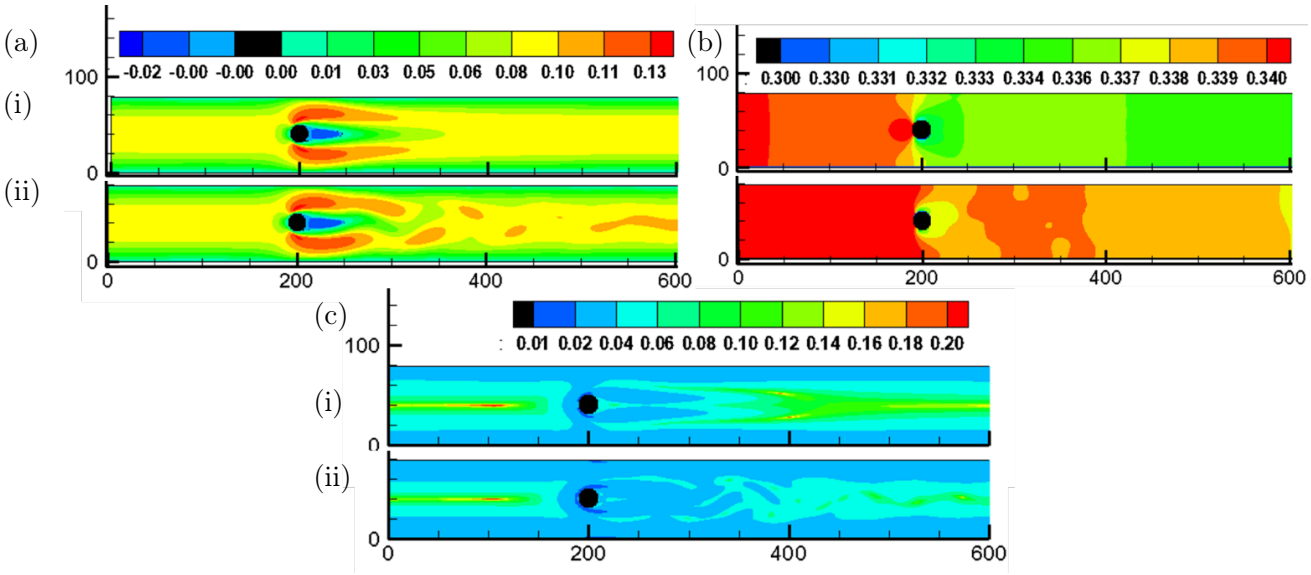

Figure 4: Contour plots for non-Newtonian fluid given case (i) ($n = 0.7,\ m = 0.07$) and case (ii) ($n = 0.7,\ m = 0.06$) (a) Velocity contour (b) Pressure contour (c) Viscosity contour

is observed, signifying a transition in the flow dynamics. This transition is notable, occurring within the Reynolds number range of 34.6 to 40.7, and underscores the sensitivity of the system to changes in Reynolds number. This shift from symmetry to asymmetry is a crucial observation in understanding the evolving flow dynamics in this context. In Figure 4(b), we focus on pressure contours for both case (i) and case (ii), which provide valuable insights into the pressure distribution within the flow. In case (i), a gradual pressure drop is clearly discernible, following an expected pattern. Specifically, a high-pressure zone is evident in front of the cylinder, followed by a region of lower pressure behind the cylinder. This gradual pressure decrease is characteristic of a stable and well-behaved flow, where the fluid moves predictably around the cylinder. However, in contrast, when we examine case (ii) in the same figure, we observe a markedly different scenario. The pressure contours in case (ii) exhibit non-uniform pressure variations along the flow length. This irregular pressure distribution suggests a departure from the expected behavior, indicating that the flow in case (ii) is experiencing turbulence or insta-

bility. This turbulent flow leads to non-uniform pressure patterns, which is consistent with the asymmetrical velocity contours observed in the previous analysis. These observations emphasize the impact of flow stability or instability on pressure profiles along the path of the cylinder. Figure 4(c) presents viscosity variation patterns for case (i) and (ii), and intriguingly, they mirror the trends observed in the velocity contours. This parallel behavior indicates that variations in viscosity are closely associated with the same ranges of flow instability previously identified. The correlation between viscosity patterns and flow instability underscores the intricate relationship between fluid properties and flow behavior. These findings reinforce the significance of understanding how changes in fluid viscosity can influence flow stability, a critical aspect in the study of complex fluid dynamics.

3.3 Shear-thickening fluid Flow

In our continued investigation, we directed our focus towards studying instability in the context of shear-thickening fluids. Employing the same Reynolds number, we aimed to determine the range of Reynolds numbers associated with instability in this specific type of fluid. This approach allowed us to pinpoint the critical Reynolds number range at which shear-thickening fluid undergoes a transition from stable to unstable flow behavior.

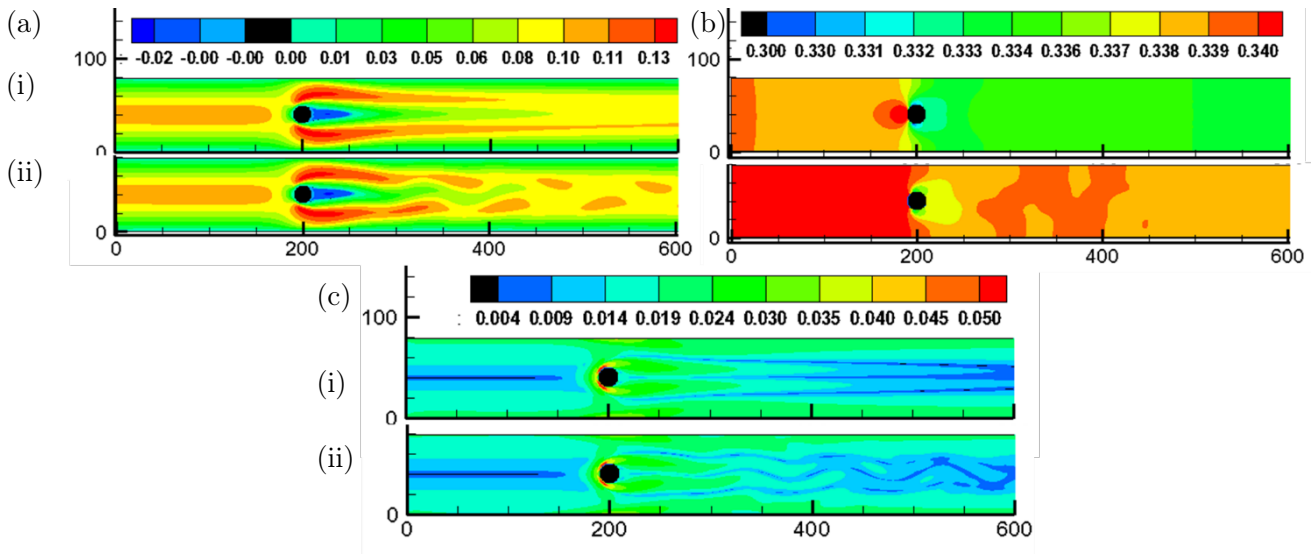

Figure 5: Contour plots for non-Newtonian fluid given case (i) ($n = 1.4,\ m = 0.17$) and case (ii) ($n = 1.4,\ m = 0.16$) (a) Velocity contour (b) Pressure contour (c) Viscosity contour

In Figure 5(a), we present velocity contours for both case (i) and case (ii), revealing a distinct pattern in the range of flow instability occurring between Reynolds numbers of 77 to 82.9. This instability is evident through asymmetry and irregularity in the flow profiles, indicative

	Given		Calculated	
Case	n	m	Re	ΔP
(i)	1.4	0.17	77	-0.0057
(ii)	1.4	0.16	82.9	-0.012

Table 4: Defining the case study with the symbol A and B form different viscosity. Case (i): $n = 1.4, m = 0.17$, Case (ii): $n = 1.4, m = 0.16$

of a transition from stable to unstable flow conditions. Interestingly, Figure 5(c) depicting viscosity contours mirrors this instability trend, further emphasizing the connection between fluid properties and flow behavior. Additionally, Figure 5(b) showcases pressure contours, where we observe irregularities in case B, corresponding to the flow instability noted earlier. This non-uniform pressure distribution aligns with the asymmetrical velocity contours and underscores the turbulent nature of the flow in this specific Reynolds number range. These findings collectively underscore the interplay between fluid properties, flow instability, and pressure patterns. They enhance our understanding of how changes in Reynolds number and fluid viscosity can influence flow behavior, providing valuable insights into complex fluid dynamics, particularly in the context of shear-thickening fluids.

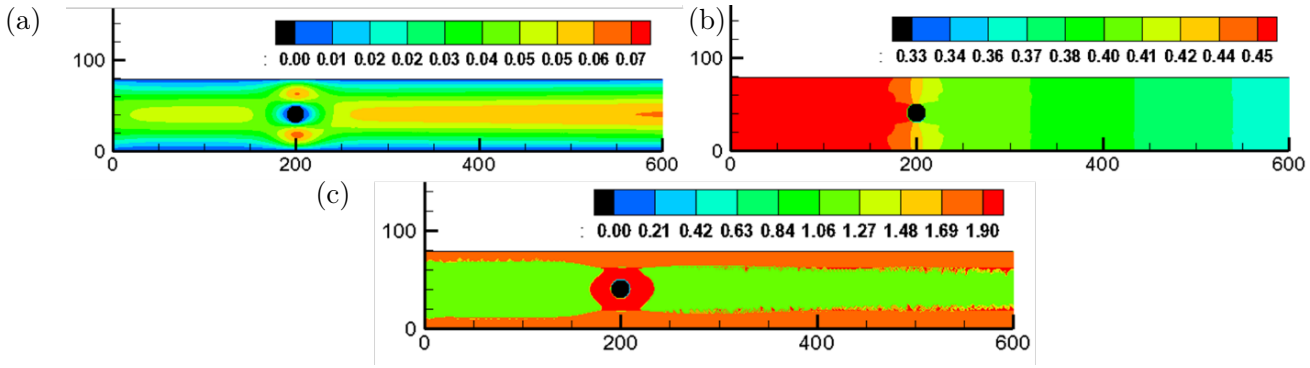

Figure 6: Contour plots for non-Newtonian fluid given case ($n_1 = 0.9,\ m_1 = 0.8$) and ($n_2 = 1.2,\ m_2 = 2.8$) (a) Velocity contour (b) Pressure contour (c) Viscosity contour

Figure 6 presents a case study involving a combination of shear thinning and shear thickening fluids with specific parameters denoted as ($n_1 = 0.9,\ m_1 = 0.8$, and $n_2 = 1.2,\ m_2 = 2.8$), respectively. The findings in Figure 6 provide valuable insights into the flow behavior in this scenario. In Figure 6(a), it is evident that the velocity of the fluid is notably higher in the vicinity of the cylinder. This observation, as depicted in Figure 6(a), signifies an increased fluid velocity near the cylinder.

Figure 6(b) illustrates changes in pressure, showcasing a gradual variation in pressure levels.

There is a distinct high-pressure region in front of the cylinder and a corresponding low-pressure zone behind the cylinder. This pressure distribution suggests that there are strong forces acting in the forward direction, while weaker forces prevail behind the cylinder. Figure 6(c) highlights variations in viscosity around the cylinder. Notably, the viscosity of the fluid is higher in the immediate vicinity of the cylinder, as demonstrated in Figure 6(c).

These findings collectively provide a comprehensive understanding of the flow dynamics and fluid properties in the case study involving a combination of shear thinning and shear thickening fluids. The distinct patterns of velocity, pressure, and viscosity distribution help elucidate the complex behavior of these fluids in this particular scenario.

3.4 Real Shear-thickening fluid Flow

In our research, we delved deeply into the intricate interplay between viscosity and strain rate in real shear-thickening fluids (STFs). To capture this intricate relationship, we employed two empirical equations: $\nu = 580.5\gamma + 0.3157$ and $\nu = -8.549\gamma + 1.6339$. These equations served as tools for modeling how the viscosity of real STFs responds to variations in applied strain rate, a critical factor in comprehending the flow characteristics of these distinctive fluids. Moreover, our investigation extended to the analysis of fluid flow in the vicinity of a cylindrical section, a geometry commonly encountered in diverse engineering contexts. We can see high viscosity at the walls and lower at the inside of the channel. Depicting a stable flow with no flow separation.

We tried to increase the average flow velocity the results are shown in figure . Notably, our findings unveiled the presence of a choking effect near the cylinder. This discovery underscores the complex and dynamic nature of real shear-thickening fluids when exposed to diverse geometric configurations.

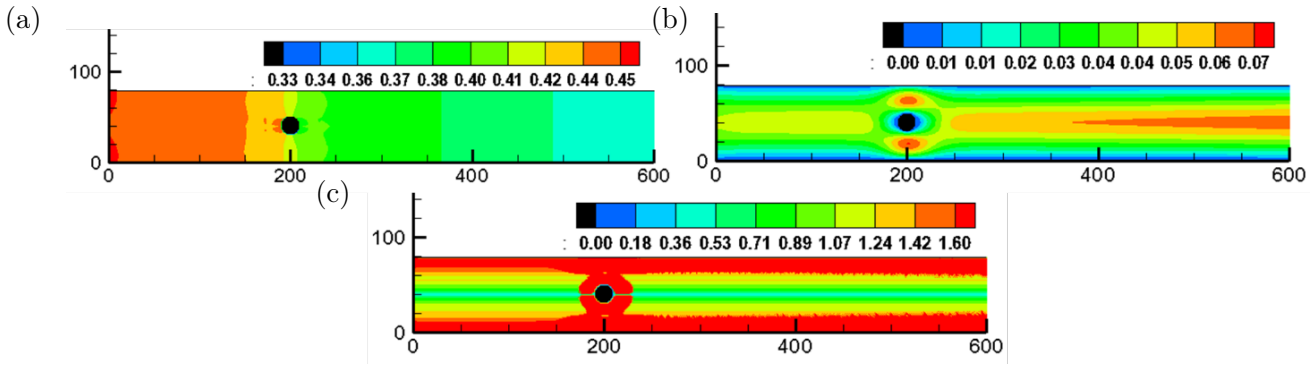

Figure 7: Contour plots for non-Newtonian fluid given case (a) Velocity contour (b) Pressure contour (c) Viscosity contour

Understanding the occurrence of this choking phenomenon holds paramount significance, as

it provides valuable insights into the flow behavior of real shear-thickening fluids in practical scenarios. These insights may have far-reaching implications for engineering and industrial applications such as bullet proof jackets, impact absorbing sports kit.

3.5 Comparison of velocity profiles of the above fluid flows at various axial locations

The velocity profiles of fluids with different rheological behaviors, such as Newtonian, shear thinning, shear thickening, and real shear thickening fluids, exhibit distinct patterns in a channel. Here's a general comparison of how velocity profiles vary at various axial locations in the channel is shown in Figure 8, respectively.

For Newtonian Fluid, we find that in the wake flow behind a cylinder ($x_1 > 200$ lu), we observe a recirculation region with a well-defined vortex shedding pattern, which remains consistent along the axial direction showing but slowly diminishing the characteristic vortex shedding and recirculation. On the other hand for shear thinning fluid flow for flow before the cylinder upto ($x_1 = 200$ lu), the flow characteristics are same as the Newtonian flow. However, Shear thinning fluids exhibited a less intense vortex shedding pattern compared to Newtonian fluids as shown with the Magenta color in Figure 8(b). This suggest the shear thinning effect can lead to changes in the size and shape of the recirculation region. Further, along the axial direction the characteristic vortex shedding and recirculation slowly diminishes as similar to the Newtonian flow.

On the other hand, the Shear thickening fluids show a more intense vortex shedding pattern with changes in the size and strength of the recirculation region compared to Newtonian and thinning fluids as shown with yellow and magenta color lines in Figure 8(c). Different axial positions reveal alterations in the intensity and structure of the vortices which diminishes as similar to the Newtonian and thinning flow.

Real shear thickening fluids exhibit a combination of shear thinning and shear thickening behavior, leading to complex changes in the wake flow pattern. Due to low shear rates, we find thinning behaviour near the centerline of the channel (i.e., in the core) of the flow where the cylinder is placed. Due to that, the vortex shedding and recirculation is less intense as compare to the power-law Shear Thickening Fluid (STF) and Newtonian flows as shown in 8(d). Further, depending on the magnitude of the shear rate and the viscosity, these vortex shedding and recirculation magnitudes are more or less intense as compared to the power-law Shear Thinning Fluid. Further, the velocity profiles at various axial locations over the cylinder may display intricate variations, influenced by the interplay between shear thinning and shear thickening characteristics of the Real Shear Thickening Fluid.

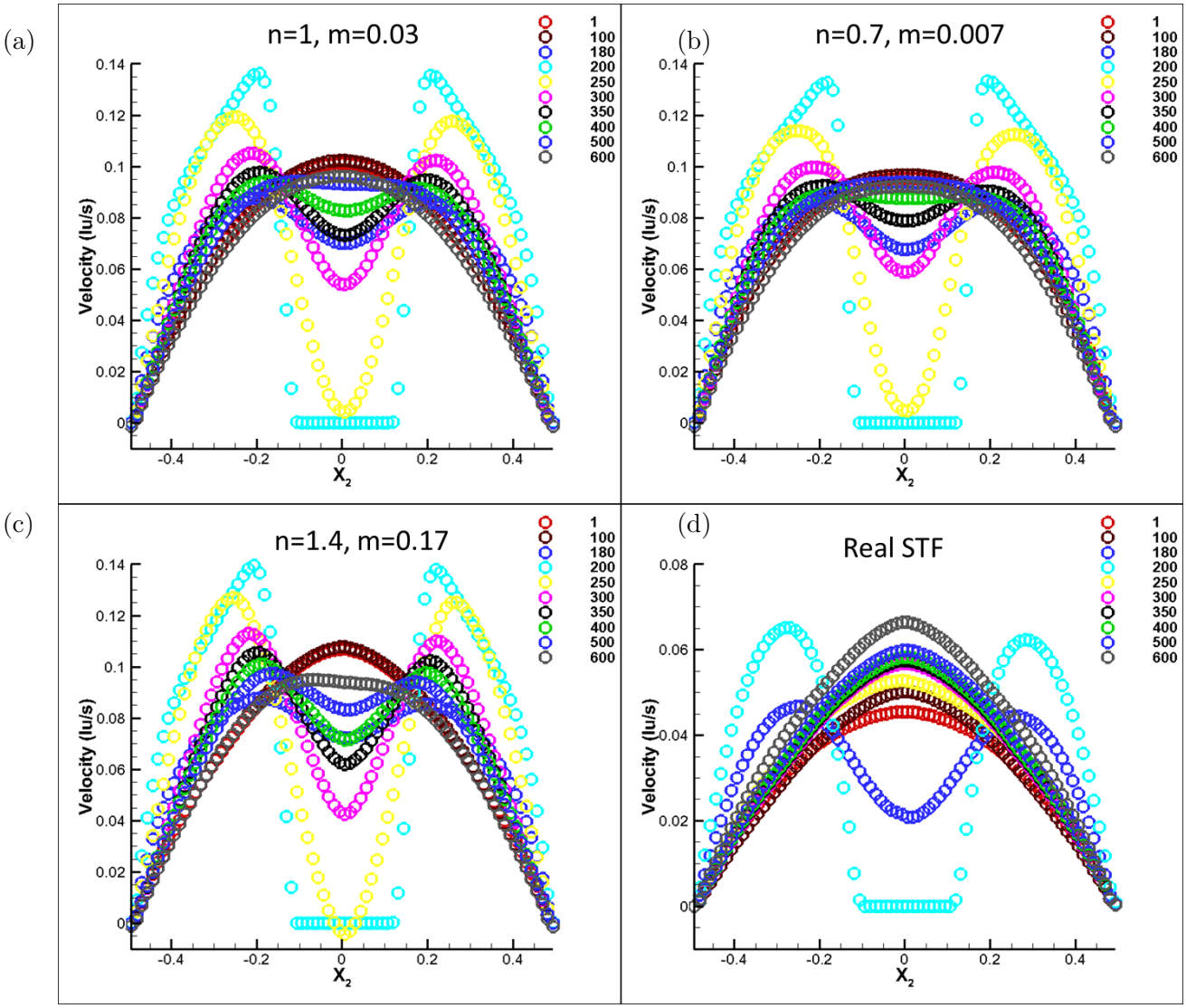

Figure 8: Velocity profiles at various axial locations for (a) Newtonian fluid flow, (b) shear thinning, (c) shear thickening, and (d) real shear thickening fluids, respectively.

3.6 Comparison of coefficient of pressure (C_p) on the surface of the cylinder for the above mentioned fluid flows

In Figure 9, we compare the pressure distribution on the circular cylinder due to Newtonian, Shear thinning, Shear thickening fluid flow using LBM studies which has a Reynolds number in the range of order $Re \sim O(10^2)$, and the literature Wu et. al. for which the $Re = 10446$, and the blockage ratio is 18.2% along with the potential fluid flow, i.e., $C_p = 1 - 4\sin^2(\theta)$ at $Re = 1.86 \times 10^5$ [24].

At the forefront of the cylinder, a stagnation point arises, causing the incoming flow to

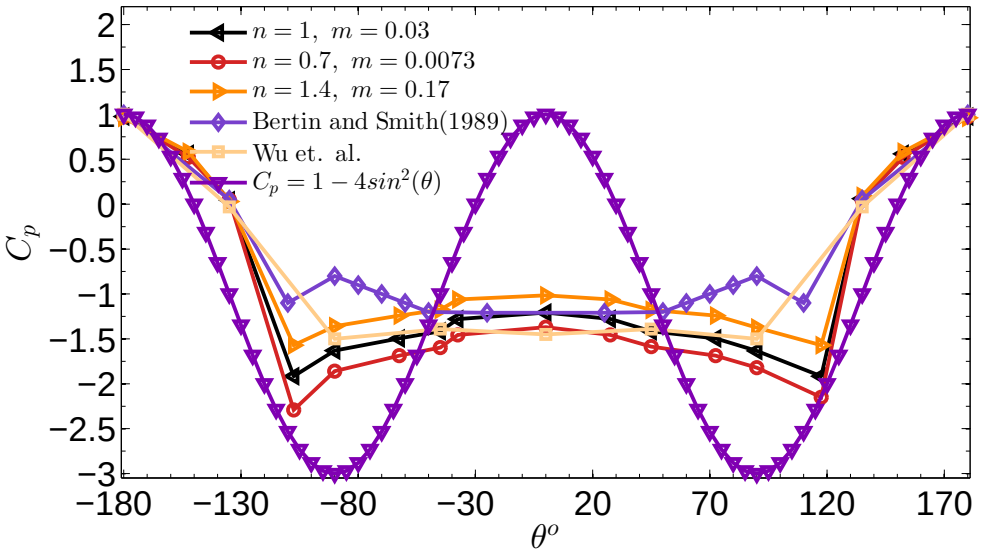

Figure 9: Comparison of pressure distribution on the circular cylinder due to Newtonian, Shear thinning, Shear thickening fluid flow using LBM studies, and the literature Wu et al. [25] and Bertin and Smith [24] along with potential fluid flow, i.e., $C_p = 1 - 4\sin^2(\theta)$.

come to a halt. The pressure at this location equals the stagnation pressure. Consequently, the pressure coefficient $C_p = 2(p_{\text{cylinder}}(\theta) - p_{\text{centreline}})/(\rho_{\text{centreline}} U^2_{\text{centreline}})$, where C_p and $p_{\text{cylinder}}(\theta)$ refer to the pressure coefficient and the pressure value at a certain angle on the cylinder, which is equivalent to 1, as per Bernoulli's principle as shown in Figure 9 for all flows at $\theta = \pm 180^o$. Also, from the inviscid, incompressible, potential theory, the pressure coefficient for the flow on the cylinder is given by $C_p = 1 - 4\sin^2(\theta) = 1$ at $\theta = \pm 180^o$ [24, 26].

When the Reynolds number based on diameter is below approximately $Re = 4 \times 10^5$, the boundary layer maintains its laminar flow from the stagnation point at the front of the cylinder to the point of separation. The resulting flow is termed subcritical, with a coefficient of drag (C_d) around 1.2. The laminar boundary layer separates just before reaching the maximum thickness across flow, as shown in previous Figures 2-6. This separation occurs because the boundary layer anticipates the deceleration of the flow, and consequently, a positive pressure gradient, that would otherwise occur on the rearward face of the cylinder.

Downstream of the separation point, the flow rapidly transitions to a turbulent state, forming a broad wake. The wake, as a whole, exhibits instability and rolls up into vortices that are shed in an antisymmetric manner at regular intervals from the cylinder, known as a von Kármán vortex street, as described by von Kármán (1963).

In case of potential flow there is no separation of flow. But in real scenario for Newtonian

and non-Newtonian flows, due to the separation, the pressure remains consistently low over the rearward face of the cylinder, leading to a net imbalance of pressure forces on the cylinder, as depicted in Figure 9, where the $C_p \sim -1.5$. We find that from our LBM studies that at the rearward of the cylinder, the $C_p \sim -1.5$ for shear thinning fluid, $C_p \sim -1.25$ for Newtonian fluid, and $C_p \sim -1$ for shear thickening fluid, these numbers are approximately similar to what we found in the compared litreture. We also find that as there is no separation of flow in potential flow theory, therefore $C_p = 1$ at $\theta = 0^o$.

Further near $\theta = \pm\ 80^o$, the flow accelerates more for thinning fluid in comparison to Newtonian and least for the thickening fluids which could also be interpret from the calculations of the $C_p = -2.2$, indicating a more negative value for thinning fluids compared to both Newtonian ($C_p = -2$) and thickening ($C_p = -1.7$) fluids. However from the potential flow theory, it reaches approximately $C_p \approx -3$ at $\theta = \pm\ 80^o$.

4 Conclusions

In this paper, we study the shear thinning, Newtonian, power-law shear thickening and the Real Shear Thickening Fluid (STF) Flow around a Circular Cylinder in uniform rigid Channels using the Lattice Boltzmann Study and compared the flow characteristics with the potential flow theory.

Real Shear Thickening Fluids (STFs) have a complex viscosity-shear rate profile, combining features of both Newtonian and non-Newtonian behavior, encompassing regions of shear thinning and shear thickening. Investigating the flow dynamics of STFs, especially in confined spaces and intricate geometries, is essential for advancing impact-resistant systems. In our exploration of these characteristics, we utilized the Lattice Boltzmann method (LBM) within a D2Q9 framework for mesoscopic numerical simulations.

Our study specifically delved into the flow behavior of an actual shear thickening fluid as it interacts with the flow past a cylinder. We thoroughly examined velocity and pressure profiles to discern the impact of real STFs. Our focus centered on understanding the real STF effects near the cylinder and how these effects vary with changes in the Reynolds number.

We find that Shear thinning fluids exhibited a less intense vortex shedding pattern compared to Newtonian fluids. On the other hand, the Shear thickening fluids show a more intense vortex shedding pattern with changes in the size and strength of the recirculation region compared to Newtonian and thinning fluids. Further, Real shear thickening fluids exhibit a combination of shear thinning and shear thickening behavior, leading to complex changes in the wake flow pattern. Due to low shear rates, we find thinning behaviour near the centerline of the channel (i.e., in the core) of the flow where the cylinder is placed. Due to that, the vortex shedding and recirculation is less intense as compare to the power-law Shear Thickening Fluid (STF) and

Newtonian flows.

We also computed the pressure coefficient on the circular cylinder in our studies and compared in with few literature with wake flow and the potential flow theory. In case of Newtonian fluid potential flow there is no separation of flow at the rearward of the cylinder. But in real viscous scenario for Newtonian and non-Newtonian flows, due to the separation, the pressure remains consistently low over the rearward face of the cylinder, leading to a net imbalance of pressure forces on the cylinder which forms the drag. We find that from our LBM studies that at the rearward of the cylinder, the $C_p \sim -1.5$ for shear thinning fluid, $C_p \sim -1.25$ for Newtonian fluid, and $C_p \sim -1$ for shear thickening fluid, these numbers are approximately similar to what we found in the compared literature. We also find that as there is no separation of flow in potential flow theory, therefore $C_p = 1$ at $\theta = 0^o$. This suggests that the thinning flow with wake creates more pressure drag which consist major portion of the total drag and less skin friction drag due to low viscosity values as compared to the Newtonian or thickening fluids. The same happens with the Real shear thickening fluid flow as it act as a thinning fluid near centreline of the channel.

In conclusion, our numerical simulation approach offers a comprehensive understanding of the subtle flow patterns exhibited by Newtonian and non-Newtonian Fluids in the context of flow past a cylinder. These insights have a significant importance in practical applications.

References

[1] Mansi Singh, Sanjeev K Verma, Ipsita Biswas, and Rajeev Mehta. Effect of molecular weight of polyethylene glycol on the rheological properties of fumed silica-polyethylene glycol shear thickening fluid. *Materials Research Express*, 5(5):055704, 2018.

[2] Liang-Liang Sun, Dang-Sheng Xiong, and Cai-Yun Xu. Application of shear thickening fluid in ultra high molecular weight polyethylene fabric. *Journal of applied polymer science*, 129 (4):1922–1928, 2013.

[3] Swarna, Sudip Kumar Pattanayek, and Anup Kumar Ghosh. Dynamic shear rheology of colloidal suspensions of surface-modified silica nanoparticles in peg. *Journal of Nanoparticle Research*, 20:1–19, 2018.

[4] RP Chhabra, AA Soares, and JM Ferreira. Steady non–newtonian flow past a circular cylinder: a numerical study. *Acta Mechanica*, 172(1-2):1–16, 2004.

[5] Sudheer Bijjam and Amit Kumar Dhiman. Cfd analysis of two-dimensional non-newtonian power-law flow across a circular cylinder confined in a channel. *Chemical Engineering Communications*, 199(6):767–785, 2012.

[6] Ram Prakash Bharti, RP Chhabra, and V Eswaran. Effect of blockage on heat transfer from a cylinder to power law liquids. *Chemical Engineering Science*, 62(17):4729–4741, 2007.

[7] Mehmet Sahin and Robert G Owens. A numerical investigation of wall effects up to high blockage ratios on two-dimensional flow past a confined circular cylinder. *Physics of fluids*, 16(5):1305–1320, 2004.

[8] Ram Prakash Bharti, RP Chhabra, and V Eswaran. Two-dimensional steady poiseuille flow of power-law fluids across a circular cylinder in a plane confined channel: wall effects and drag coefficients. *Industrial & engineering chemistry research*, 46(11):3820–3840, 2007.

[9] Jyoti Chakraborty, Nishith Verma, and RP Chhabra. Wall effects in flow past a circular cylinder in a plane channel: a numerical study. *Chemical Engineering and Processing: Process Intensification*, 43(12):1529–1537, 2004.

[10] Luigino Zovatto and Gianni Pedrizzetti. Flow about a circular cylinder between parallel walls. *Journal of Fluid Mechanics*, 440:1–25, 2001.

[11] Eric SG Shaqfeh. Purely elastic instabilities in viscometric flows. *Annual Review of Fluid Mechanics*, 28(1):129–185, 1996.

[12] Raj P Chhabra and John Francis Richardson. *Non-Newtonian flow in the process industries: fundamentals and engineering applications*. Butterworth-Heinemann, 1999.

[13] D Arumuga Perumal, Gundavarapu VS Kumar, and Anoop K Dass. Lattice boltzmann simulation of viscous flow past elliptical cylinder. *CFD letters*, 4(3):127–139, 2012.

[14] Praveen Chandrashekar and Ashish Garg. Vertex-centroid finite volume scheme on tetrahedral grids for conservation laws. *Computers & Mathematics with Applications*, 65(1):58–74, 2013.

[15] Amir Nejat, Vahid Abdollahi, and Koohyar Vahidkhah. Lattice boltzmann simulation of non-newtonian flows past confined cylinders. *Journal of Non-Newtonian Fluid Mechanics*, 166(12-13):689–697, 2011.

[16] A Grucelski and J Pozorski. Lattice boltzmann simulations of flow past a circular cylinder and in simple porous media. *Computers & Fluids*, 71:406–416, 2013.

[17] YY Yan and YQ Zu. Numerical simulation of heat transfer and fluid flow past a rotating isothermal cylinder–a lbm approach. *International Journal of Heat and Mass Transfer*, 51 (9-10):2519–2536, 2008.

[18] Keivan Fallah, Morteza Khayat, Mohammad Hossein Borghei, Atena Ghaderi, and Ehsan Fattahi. Multiple-relaxation-time lattice boltzmann simulation of non-newtonian flows past a rotating circular cylinder. *Journal of Non-Newtonian Fluid Mechanics*, 177:1–14, 2012.

[19] Manju Bisht and Dhiraj V Patil. Assessment of multiple relaxation time-lattice boltzmann method framework for non-newtonian fluid flow simulations. *European Journal of Mechanics-B/Fluids*, 85:322–334, 2021.

[20] Saad Adam and Kannan N Premnath. Numerical investigation of the cascaded central moment lattice boltzmann method for non-newtonian fluid flows. *Journal of Non-Newtonian Fluid Mechanics*, 274:104188, 2019.

[21] Garima Vishal, Ashish Garg, Jayati Sarkar, and Sudip K Pattanayek. The channel flow of a real shear thickening fluid using the lattice boltzmann simulation and the theoretical model. *ChemRxiv- Chemical Engineering and Industrial Chemistry, DOI: 10.26434/chemrxiv-2023-zk1nn*, pages 1–26, 2023.

[22] Garima Vishal, Ashish Garg, Jayati Sarkar, and Sudip Kumar Pattanayek. Real shear thickening fluid (stf) flow in converging-diverging channels: Analytical and lattice boltzmann study. *ChemRxiv- Chemical Engineering and Industrial Chemistry, DOI: 10.26434/chemrxiv-2023-3cjvq*, pages 1–29, 2023.

[23] Garima Vishal, Jyoti Tomar, and Ram Prakash Bharti. Critical parameters for non-newtonian shear-thickening power-law fluids flow across a channel confined circular cylinder. *Journal of the Taiwan Institute of Chemical Engineers*, 123:34–46, 2021.

[24] JJ Bertin and ML Smith. *Aerodynamics for Engineers—Second Edition*. Cambridge University Press, 1989.

[25] Bo Wu, Yantao Yin, Mei Lin, Liangbi Wang, Min Zeng, and Qiuwang Wang. Mean pressure distributions around a circular cylinder in the branch of a t-junction with/without vanes. *Applied thermal engineering*, 88:82–93, 2015.

[26] Ashish Garg. Aerodynamics. In *GATE Aerospace Forum Educational Services*, 2015.